Journal of Ovarian Research

RESEARCH

Open Access

LCK facilitates DNA damage repair by stabilizing RAD51 and BRCA1 in the nucleus of chemoresistant ovarian cancer

Goutam Dey[1†], Rashmi Bharti[1†], Chad Braley[1], Ravi Alluri[1], Emily Esakov[1], Katie Crean-Tate[2], Keith McCrae[1,3], Amy Joehlin-Price[4], Peter G. Rose[2], Justin Lathia[1,3], Zihua Gong[3,5] and Ofer Reizes[1,3*]

Abstract

Poly-ADP Ribose Polymerase (PARP) targeted therapy is clinically approved for the treatment of homologous recombination (HR) repair deficient tumors. The remarkable success of this therapy in the treatment of HR repair deficient cancers has not translated to HR-proficient cancers. Our studies identify the novel role of non-receptor lymphocyte-specific protein tyrosine kinase (LCK) in the regulation of HR repair in endometrioid epithelial ovarian cancer (eEOC) model. We show that DNA damage leads to direct interaction of LCK with the HR repair proteins RAD51 and BRCA1 in a kinase dependent manner RAD51 and BRCA1 stabilization. LCK expression is induced and activated in the nucleus in response to DNA damage insult. Disruption of LCK expression attenuates RAD51, BRCA1, and BRCA2 protein expression by hampering there stability and results in inhibition of HR-mediated DNA repair including suppression of RAD51 foci formation, and augmentation of γH2AX foci formation. In contrast LCK overexpression leads to increased RAD51 and BRCA1 expression with a concomitant increase in HR DNA damage repair. Importantly, attenuation of LCK sensitizes HR-proficient eEOC cells to PARP inhibitor in cells and pre-clinical mouse studies. Collectively, our findings identify a novel therapeutic strategy to expand the utility of PARP targeted therapy in HR proficient ovarian cancer.

[†]Goutam Dey and Rashmi Bharti are co-first authors.

*Correspondence:
Ofer Reizes
reizeso@ccf.org
Full list of author information is available at the end of the article

Graphical Abstract

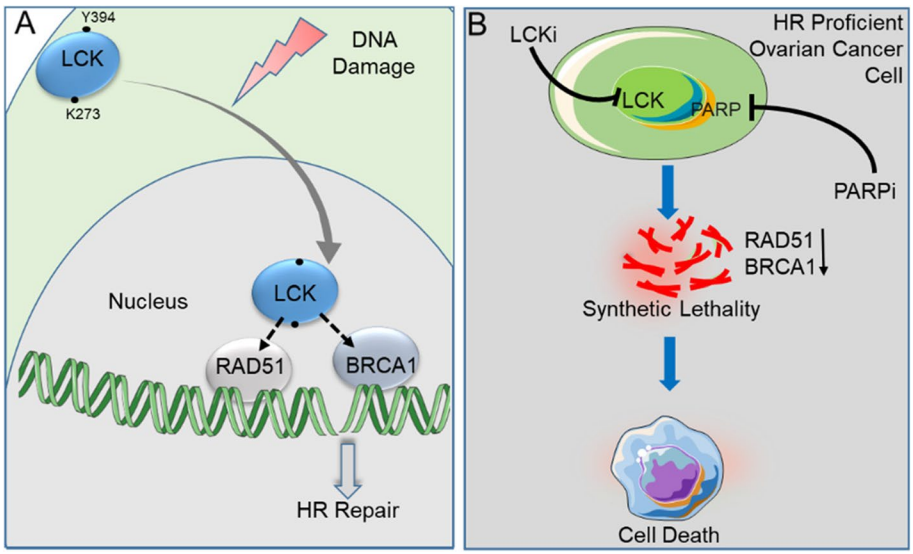

Introduction

Epithelial ovarian cancer (EOC) is the second most common gynecologic malignancy in the United States, but the leading cause of gynecologic cancer death. It is estimated that in 2023, ~ 19,710 women in the U.S. will be diagnosed with epithelial ovarian cancer (EOC) and 13,270 will die from their disease [1]. Poly-(ADP-ribose) polymerase inhibitors (PARPi) have emerged as new therapeutic options in the treatment of ovarian cancer [2–4]. Recent studies show that this treatment has prolonged median recurrence-free survival after primary therapy by more than 24 months [5]. While the benefit of PARPi is greatest in *BRCA1/2*-mutant or deficient tumors, those with HR deficiencies also experience a benefit from this therapy [5]. Conversely, PARPi and chemotherapy have so far shown limited efficacy in HR-proficient ovarian cancers [6]. Further, platinum resistance is associated with HR proficiency in EOC [7, 8]. This limited efficacy of both platinum and PARPi therapy highlights an unmet clinical need in ovarian cancer patients.

Several strategies have been assessed to expand the utility of PARPi in HR-proficient cancers [2, 9–11]. As RAD51, BRCA1, and BRCA2 are critical components of the HR repair complex, studies have focused on disrupting this complex [12]. Cyclin-dependent kinase (CDK) proteins were shown to regulate the HR repair pathway in a lung cancer model [13]. The CDK inhibitor dinaciclib can attenuate the expression of RAD51 and BRCA proteins resulting in the inhibition of HR repair capacity and potentiation of the pharmacological effect of PARPi [10]. However, there is no clinically approved drug for combination with PARPi for HR-proficient cancers.

Approximately 80% of endometrial cancers and 10% of ovarian cancers demonstrate endometrioid tumor histology (eEOC) [14]. A small but clinically significant proportion of eEOC display high-grade histology, advanced stage (FIGO stage III-IV), and a poor 5-year survival of 6–24%. These traits are like those of the more aggressive high-grade serous type of ovarian cancer [15]. Moreover, somatic and/or germline mutations in HR genes including *BRCA1/2* occur in only a third of ovarian tumors, indicating the majority of eEOC are HR-proficient. Of note, eEOC show a considerably higher rate of resistance to platinum-based chemotherapy compared to serous carcinomas and do not commonly respond to targeted therapies such as PARP inhibitors [16].

We previously determined that the intracellular, non-receptor tyrosine kinase, LCK regulates genes implicated in DNA repair machinery in eEOC [17]. We also demonstrated the pharmacologic inhibition of LCK attenuated expression of homologous recombination DNA damage repair genes leading to sensitization of eEOC cells to cisplatin [18]. In contrast, increased expression of LCK led to upregulation of DNA damage-repair genes and increased resistance to cisplatin. As LCK modulates RAD51, BRCA1, and BRCA2 expression, we hypothesized that blocking LCK expression or inhibiting kinase activity would sensitizes eEOC to PARPi. Here, we elucidate the mechanism of LCK in regulating HR DNA

damage repair and identify a therapeutic approach to sensitize HR-proficient eEOC to PARP inhibitors.

Results

LCK complexes with RAD51 and BRCA1 in response to DNA damage in an LCK kinase dependent manner

We tested whether LCK directly interacts with RAD51 and BRCA1 in nuclear extracts. For this, CP70 and SKOV3 cells were transduced with a myc-tagged LCK treated cells with/without etoposide, isolated nuclei, and performed an IP (immunoprecipitation) assay with myc antibodies (Fig. 1A and Supplementary Fig. S1). CP70 and SKOV3 ovarian cancer cells are cisplatin resistant endometrioid ovarian cancer models [19].

In untreated cells, neither BRCA1 nor RAD51 co-precipitated with mycLCK. In contrast, etoposide treatment resulted in co-precipitation of RAD51 and BRCA1 with mycLCK (Fig. 1B,C). In parallel, RAD51 could co-immunoprecipitate LCK from etoposide-treated SKOV3 OE cells. LCK and BRCA1 were detected in RAD51 immunoprecipitates (Fig. 1D).

We next tested whether kinase activity and autophosphorylation of LCK is necessary for BRCA1 and RAD51 co-immunoprecipitation in response to DNA damage. We generated LCK mutants at lysine 273 (K273R), necessary for catalytic activity; tyrosine 394 (Y394F), necessary for autophosphorylation and activation [20]; and tyrosine 192 (Y192F), the SH2 adaptor protein binding site [21]. Mutants were transduced into LCK KO CP70 cells. OE and Y192F mutants retained kinase activity, while K273R and Y394F mutants lacked kinase activity. We performed IP studies in etoposide-treated cells and determined that OE and Y192F cells were able to co-immunoprecipitate BRCA1 and RAD51, whereas K273R and Y394F failed to co- immunoprecipitate BRCA1 and RAD51 (Fig. 1E). These findings indicate that in response to DNA damage, LCK with intact kinase activity interacts with a complex containing RAD51 and BRCA1 (Fig. 1F).

To test the hypothesis that LCK increases the stability of BRCA1 and RAD51 proteins, empty vector EV and OE cells were treated with cycloheximide and harvested at 0, 1, 2, 3, 5, and 6 h followed by quantification of protein expression levels (Fig. 1G,H and Supplementary Fig. S2). Half-lives of RAD51 in CP70 EV and OE cells treated with cycloheximide were 3.2 and 5.6 h, respectively. Half-lives of BRCA1 in CP70 EV and OE cells treated with cycloheximide were 54 min and 3.4 h, respectively. These studies indicate that LCK is sufficient to regulate BRCA1 and RAD51 protein expression via protein stabilization. We observed that DNA damage induction led to interaction of LCK with Rad51/BRCA1 in OC cells. Interestingly, without inducing DNA damage, LCK overexpression was sufficient to increase the stability of Rad51 and BRCA1. These findings indicated that LCK phosphorylation leads to stabilization of Rad51 and BRCA1 proteins.

LCK regulation of DNA double strand break repair

As γH2AX and RAD51 are markers of DNA damage and repair of double strand breaks, we tested for foci formation in control and etoposide-treated cells. LCK was overexpressed (OE) in CRISPR/Cas9-background (KO) cells and treated in absence or presence of etoposide then subjected to immunofluorescence analysis to detect and quantify γH2AX foci (Fig. 2A, B and Supplementary Fig. S3A). In the absence of etoposide, no γH2AX foci formation was detected. Parental CP70 (WT) cells treated with etoposide led to increased γH2AX foci compared to DMSO treatment. KO cells treated with etoposide exhibited 4–5 fold increased foci formation compared to WT. Foci formation was nearly completely blocked in etoposide treated OE cells (Fig. 2A and B). This supports the proposal that LCK is sufficient to promote double strand DNA (dsDNA) damage repair.

To further test the hypothesis, we assessed RAD51 foci formation in KO and OE CP70 cells treated in the absence or presence of etoposide (Fig. 2C, D and Supplementary Fig. S5B). As with γH2AX, no RAD51 foci were observed in WT, KO, or OE cells treated with DMSO. In contrast, etoposide treatment led to a significant increase in RAD51 foci in WT CP70 cells that was significantly suppressed in KO cells (Fig. 2C, D, and Supplementary Fig. S3B). RAD51 foci formation was significantly increased in OE cells treated with etoposide. This data supports the conclusion that LCK can regulate HR repair during dsDNA damage response (DDR).

LCK kinase activity is essential for HR repair

We next assessed γH2AX and RAD51 foci formation in OE, K273R, Y192F, and Y394F transduced cells. OE and Y192F exhibited similar level of foci formation in response to etoposide (Fig. 2E, F, G and H), whereas K273R and Y394F showed increased γH2AX foci and reduced RAD51 foci in etoposide treated cells (Fig. 2E, F, G and H and Supplementary Fig. S4). We determined the etoposide sensitivity in naïve CP70, LCK KO, LCK OE (In LCK knock out background), and LCK mutants (In LCK knock out background) cells (Fig. 2I). The IC_{50} for etoposide was 5 μM in naïve CP70 cells, 1.67 μM in LCK KO, and 10.03 μM in LCK OE and 8.70 μM for Y192F. Interestingly, K273R and Y394F showed of IC50 values of etoposide, 2.28 μM and 2.01 μM (For statistical analysis see the Supplementary table S14). Analyzing these data, we showed that LCK kinase facilities DNA damage repair during DDR. We performed a timed experiment with etoposide treated CP70 cells and determined that the

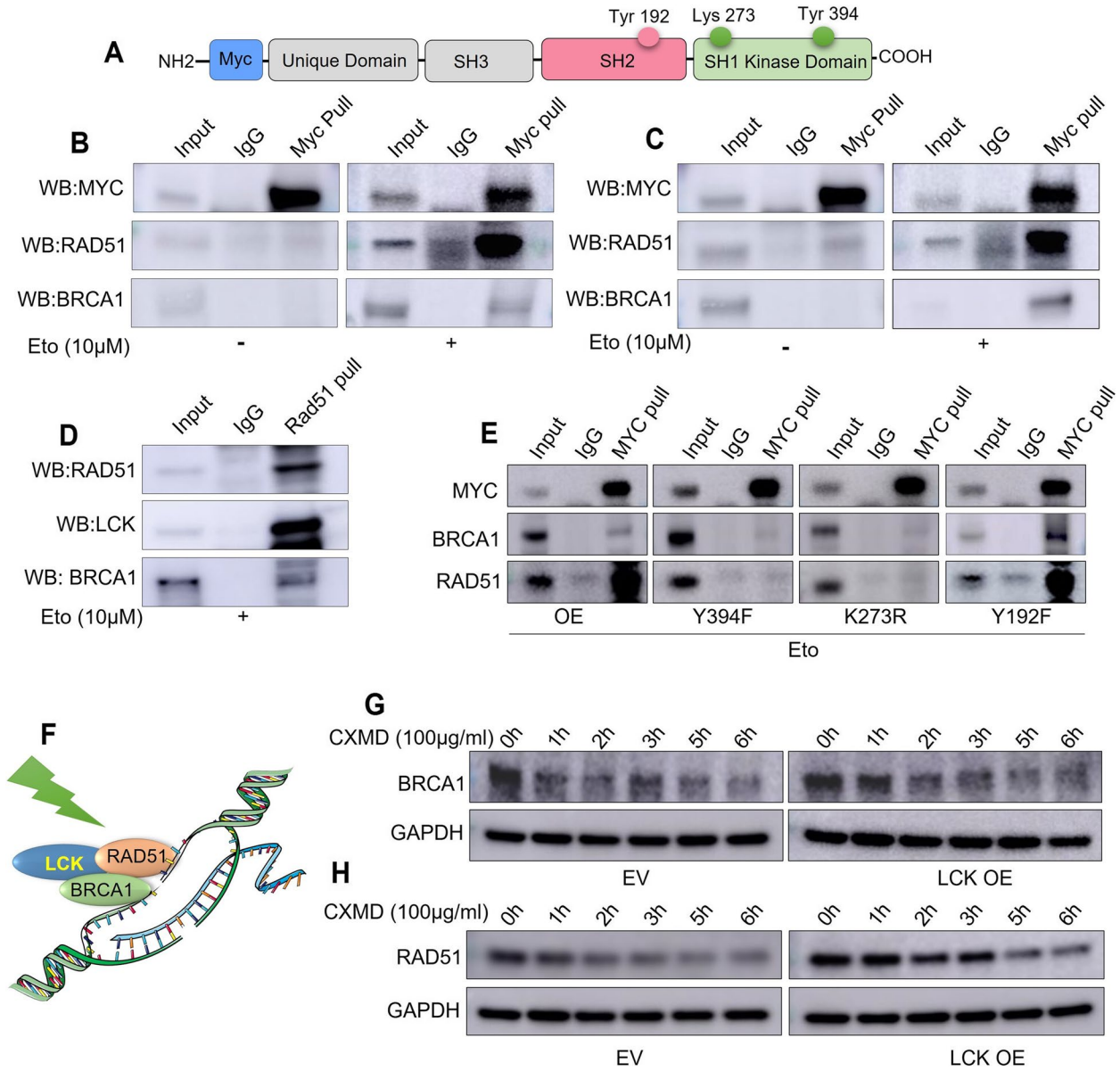

Fig. 1 LCK interacts with RAD51/BRCA1 in response to DNA damage and stabilizes RAD51/BRCA1 (**A**) Structure of MYC labelled LCK construct. LCK Y394F, LCK K273R, LCK Y192F mutants were generated by site directed mutagenesis. Mutants were transduced in CP70 cells on LCK CRISPR KO background. **B** Myc tagged LCK expressing CP70 cells were treated with vehicle (DMSO) or etoposide for 24 h, washed to remove etoposide and incubated for an additional 24 h, then harvested, lysed, and nuclei were purified. Extracts were Immunoprecipitated with Myc followed by immunoblotting for Myc, BRCA1, and RAD51. **C** Myc tagged LCK expressing SKOV3 cells were likewise treated with vehicle or etoposide. Myc protein was immunoprecipitated and immunoblotted for LCK, RAD51, and BRCA1. **D** LCK overexpressing SKOV3 cells were treated with etoposide. RAD51 was immunoprecipitated from total extracts followed by immunoblotting for LCK and RAD51. **E** CP70 cells (MYC tagged LCK, LCK Y394F, LCK K273R, and LCK Y192F) were treated with etoposide/DMSO for 24 h, washed free of Etoposide and incubated for an additional 24 h. Cells were harvested and nuclei isolated. Extracts were immunoprecipitated with MYC antibodies followed by immunoblotting for LCK, RAD51, and BRCA1 proteins. **F** Schematic of LCK binding partners in response to DNA damage. **G** CP70 EV and CP70 LCK OE cells were treated with cycloheximide over a 6 h period and extracts collected at 0, 1, 2, 3, 5, and 6 h. Cells were harvested followed by immunoblotting for RAD51 and BRCA1 protein expression. Each experiments were repeated for at least three times

extent of γH2AX foci was lower in OE and LCK Y192F mutant cells than in WT cells at 0 h. Moreover, KO, Y394F, and K273R cells exhibited the highest number of γH2AX foci at all time points (Fig. 2J, and Supplementary Fig. S5). These findings support to the hypothesis that LCK kinase activity is essential for interaction with

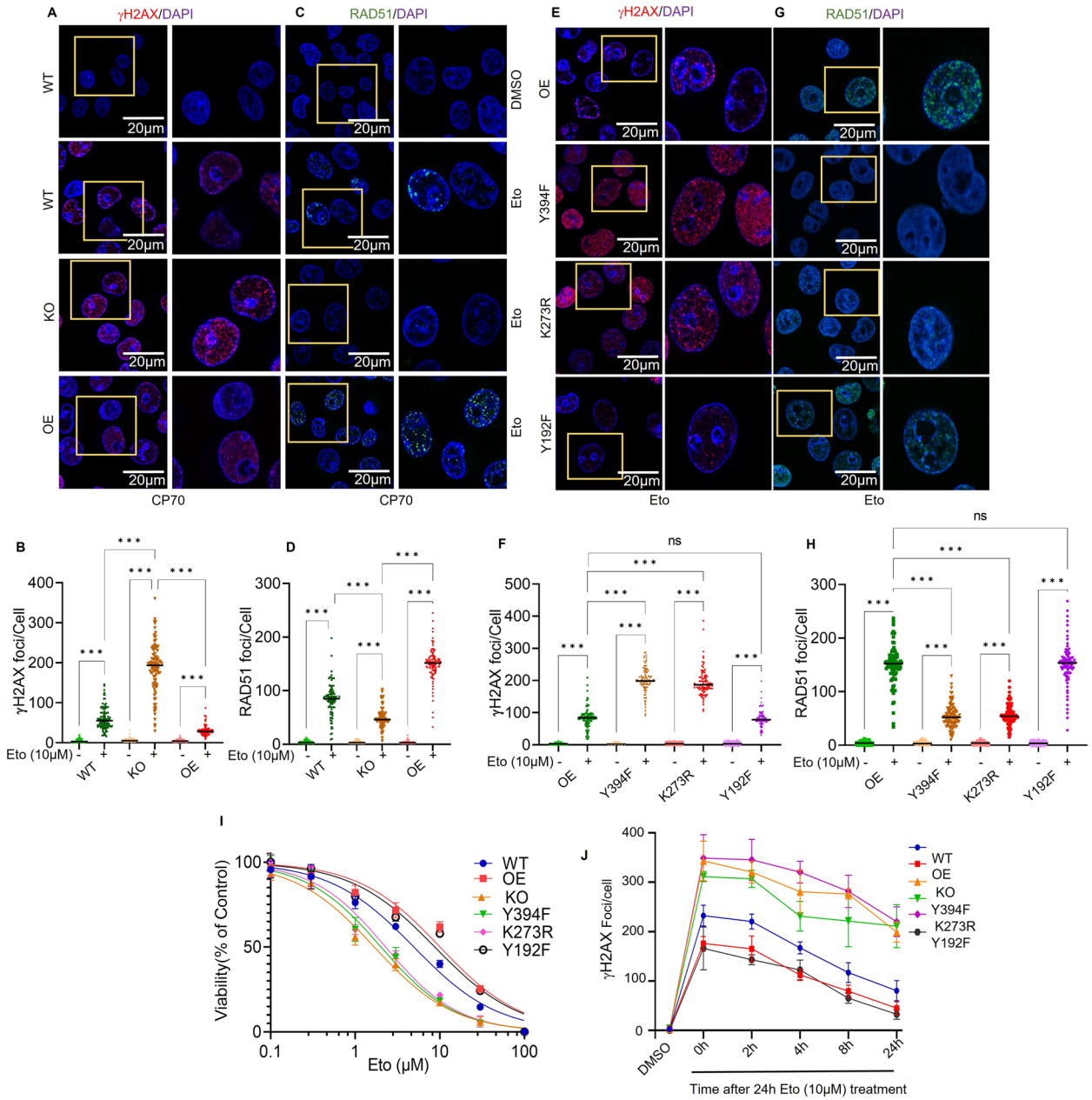

Fig. 2 LCK regulates DNA damage and repair. (**A** and **B**) CP70 WT, LCK KO via CRISPR/Cas9 (KO), and LCK OE on CRISPR background (OE) cells were treated with DMSO/etoposide 10 μM for 24 h, followed by an additional 24 h without etoposide. Immunofluorescence was performed to visualize γH2AX foci formation. Scale bar represents 10 μm. γH2AX foci were counted by image J software and 100 cells were counted and plotted. **C** and **D** CP70 WT, LCK KO via CRISPR/Cas9 (KO), and LCK OE on CRISPR background (OE) cells were treated with DMSO/etoposide 10 μM for 24 h. Cells were incubated in drug free media for another 24 h. Immunofluorescence was performed to visualize RAD51 foci formation. RAD51 foci in 100 cells were counted by image J software. **E** and **G** CP70 cells (LCK OE, LCK Y394F, LCK K273R, and LCK Y192F) were treated with etoposide for 24 h, followed by an additional 24 h without etoposide. Immunofluorescence was performed to visualize γH2AX and RAD51 foci formation. **F** and **H** RAD51 and γH2AX foci were counted on 100 representative cells by image J software and the quantification of foci was plotted in the graph. I CP70 cells (WT, LCK OE, LCK KO, LCK Y394F, LCK K273R, and LCK Y192F) were treated with increasing concentrations of etoposide for 48 h. Cell titer glow viability assays were performed to check cell viability. **J** CP70 cells (LCK, LCK Y394F, LCK K273R, and LCK Y192F in LCK knock out background) were grown on cover slips and treated with etoposide for 24 h followed by incubation for 0, 2, 4, 8 and 24 h. Cells were then subjected to immunofluorescence analysis to visualize γH2AX foci formation. γH2AX foci in 100 random cells were counted and plotted to visualize the γH2AX decay kinetics. One way ANOVA analysis was performed with Tukey's multiple comparisons test to compare different groups (* $p < 0.05$, ** $p < 0.01$, *** $p < 0.001$). Each experiment was repeated at least three times

RAD51 and BRCA1 during DNA damage response and facilitated HR repair.

DNA damage induces LCK dependent BRCA1 expression

We next assessed the effects of DNA damage on LCK expression and activation. DNA damage in ovarian cancer cells was induced using either etoposide, ultraviolet radiation, or methyl methanesulfonate (MMS). Dose-dependent treatment of CP70 cells with etoposide or MMS led to increased LCK protein expression (Fig. 3A). Etoposide or MMS treatment in SKOV3 cells led to increased phosphorylation of LCK at pY394, while total levels of LCK protein remained unchanged (Supplementary Fig. S6A). Likewise, ultraviolet radiation of CP70 cells was sufficient to increase LCK phosphorylation (Supplementary Fig. S6B). BRCA1 and γH2AX expression was induced by etoposide or MMS, indicating increased DNA damage (Fig. 3A and Supplementary Fig. S7A, B). As DNA damage, particularly double strand breaks (DSB), and its repair machinery are concentrated in the nucleus [22], we investigated the effects that DNA damage could induce on the accumulation of LCK in the nucleus. We found increased total LCK and pLCK in the nucleus of etoposide-treated cells (Fig. 3B and Supplementary Fig. S7C). Sub-cellular fractionation and immunofluorescence analysis both showed that pLCK was predominately localized in the nucleus of etoposide-treated cells (Fig. 3C). These findings were replicated in SKOV3 cells (Supplementary Fig. S6C). We assessed the expression of LCK by immunohistochemical analysis in human endometrioid ovarian tumor specimens (Fig. 3D). LCK positive tumor cells were observed and LCK protein was distributed in the cytoplasm as well as the nucleus. We next tested whether inhibition of LCK would be sufficient to block BRCA1 expression in etoposide-treated cells. Etoposide treatment in shCon cells showed increased BRCA1 protein expression, whereas this treatment attenuated BRCA1 expression in KD cells (Fig. 3E and Supplementary Fig. S7D). We repeated these studies in CRISPR/CAS9 KO cells and observed similar attenuation of BRCA1 in KO CP70 cells and no attenuation in parental cells (Fig. 3F and Supplementary Fig. S7E). These findings indicate that the induction of BRCA1 expression in response to DNA damage is disrupted by LCK inhibition. We tested whether LCK inhibition is sufficient to inhibit HR DNA repair genes *RAD51, BRCA1, and BRCA2* at the protein level. We inhibited LCK expression using shRNA and CRISPR in CP70 and SKOV3 cell lines. Cells were transduced with lentivirus containing shRNA control (shCon) or LCK-targeted shRNA (KD1, KD2). Additionally, we generated LCK knock-out (KO) CP70 cells via CRISPR/Cas9. LCK inhibition was confirmed by immunoblotting followed by analysis of expression of BRCA1, BRCA2, and RAD51 via western blot analysis. In CP70 cells, we observed that KD1, KD2, and KO displayed attenuated protein expression of BRCA1, BRCA2 and RAD51 when compared to shCon (Supplementary Fig. S8A). The protein expression levels of BRCA1, BRCA2, and RAD51 were similarly attenuated in LCK knock-down SKOV3 cells (Supplementary Fig. S8A).

In complementary studies, we tested whether LCK overexpression would increase RAD51, BRCA1, and BRCA2 protein expression in eEOC. LCK overexpression led to induction of RAD51, BRCA1, and BRCA2 protein expression in CP70 and SKOV3 cells (Supplementary Fig. S8A).

To test whether pharmacologic inhibition of LCK can attenuate expression of DNA damage repair proteins, we used PP2, a cell-permeable, small-molecule inhibitor of LCK kinase [23, 24]. We tested the efficacy of PP2 in CP70 and SKOV3 OE cells. PP2 attenuated pLCK at Y394, the autophosphorylation site of LCK in these cells (Supplementary Fig. S8B). We also observed that total LCK was attenuated. This might be due to phosphorylation of LCK effect on the stability of the LCK protein as previously published (Ana Giannini et al. Mol Cell Biol. 2004). γH2AX, a marker of DNA damage and replication stress, was elevated by PP2 treatment. This is indicative of either increased damage or reduced repair of DNA damage due to attenuation of BRCA1 and RAD51 expression. We tested whether genetic deletion of LCK would induce change in cell cycle phase (Supplementary Fig. S9). We found that there is no significant changes in G0/G1, S, and G2M population between LCK overexpression and LCK knock out groups in CP70 cells. These findings indicate that changes in BRCA1 and RAD51 are not due to cell cycle arrest. LCK inhibition also attenuates expression of RAD51, BRCA1, and BRCA2 in parental CP70 and SKOV3 as well as in the CRL1978 clear-cell EOC cell line (Supplementary Fig. S10A).

LCK inhibition attenuates HR repair efficiency

The inhibition of DNA damage repair genes led us to test whether LCK inhibition impairs HR-dependent DNA repair. We utilized the DR-GFP reporter assay established in U2OS cells to measure repair efficiency [25] (Fig. 4A). U2OS cells with/without DR-GFP reporter system express endogenous LCK protein expression as shown by western blot analysis (Supplementary Fig. S10B). U2OS cells treated with PP2 leads to a dose-dependent reduction of the GFP-positive cell population when compared to DMSO-treated cell population, indicating reduced DNA damage repair as a consequence of LCK inhibition (Fig. 4B) (Supplementary Fig. S10C). Likewise, shRNA silencing of LCK led to a reduction in the GFP-positive population compared to shCon transduced cells (Fig. 4B).

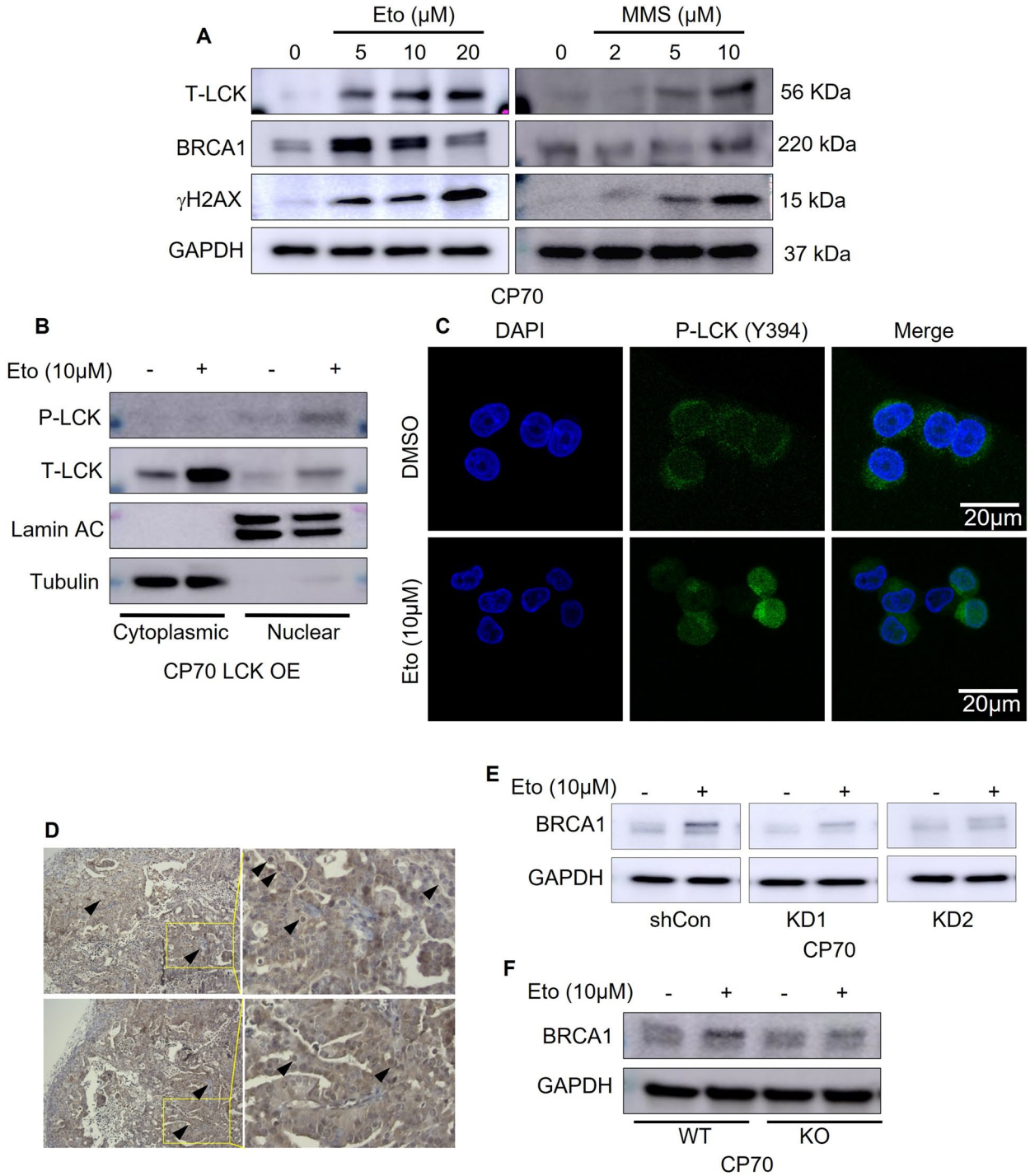

Fig. 3 pLCK is localized in nucleus in response to DNA damage and LCK disruption suppresses BRCA1 expression in response to DNA damage. **A** Western blot analysis of T-LCK, BRCA1 and yH2AX expression following 24 h etoposide or MMS treatment, followed by 24 h recovery in CP70 cells. **B** CP70 LCK OE cells were treated without or with etoposide, harvested and cytoplasmic and nuclear fractions isolated, followed by western blot analysis. **C** Immunofluorescence of pLCK in CP70 cells treated without or with etoposide. Scale bar represents 10 μm. (**D**) Human tissue samples of endometrioid ovarian cancer were processed for immunohistochemistry to detect LCK protein expression. Two representative images are shown, and the selected area is magnified. **E** CP70 cells were transduced with control shRNA (shCon) or LCK specific shRNA (KD1, KD2), treated with etoposide or without and BRCA1 expression detected by immunoblots. GAPDH served a loading control. **F** CP70 parental or LCK CRISPR KO were treated with etoposide or without and BRCA1 expression detected by immunoblots. GAPDH served a loading control. All experiments were replicated three times

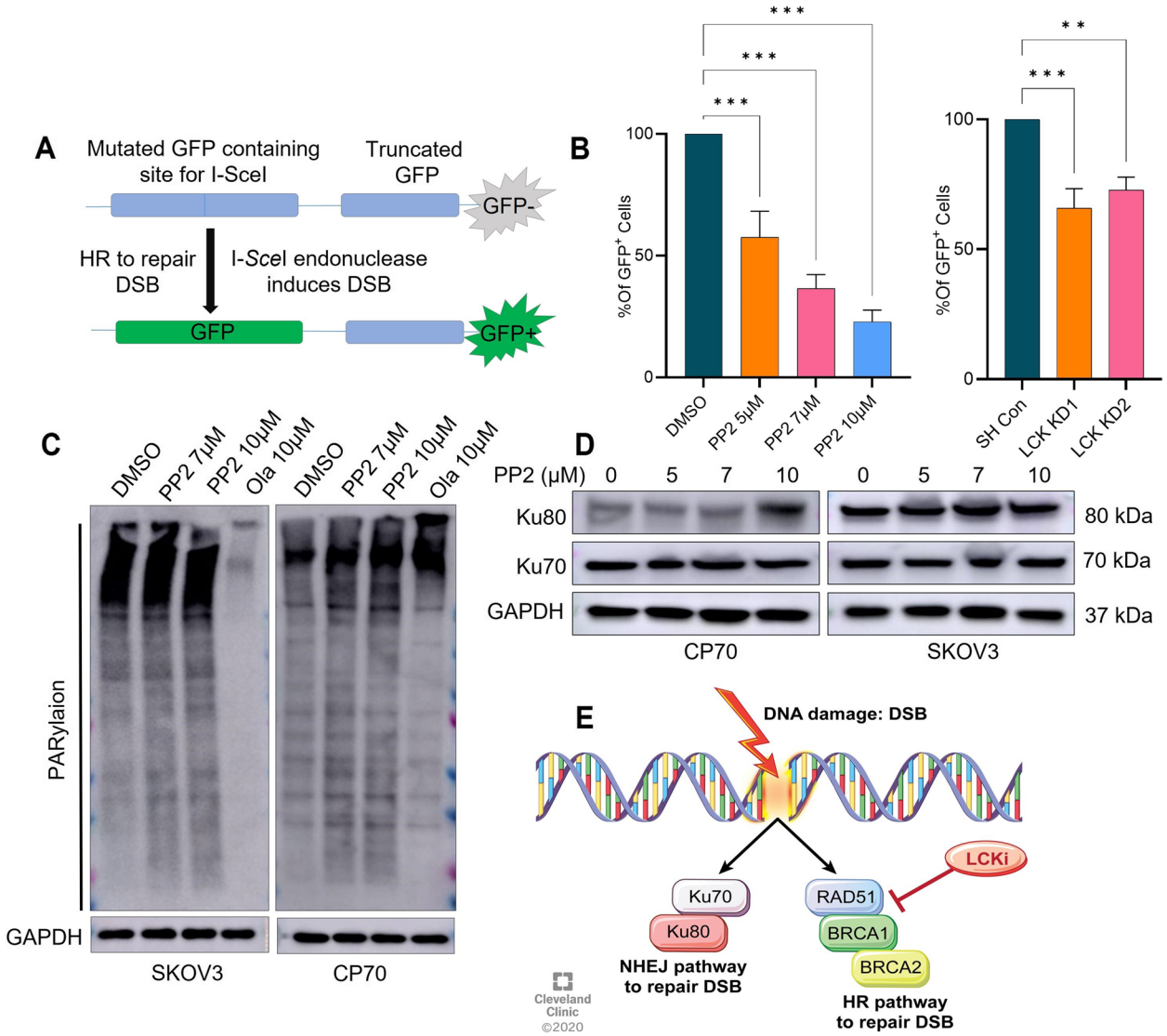

Fig. 4 LCK inhibition attenuates the HR repair pathway. **A** Schematic of DNA repair assay in U2OS osteosarcoma cells stably transduced with the DR-GFP reporter system. This reporter system contains an upstream mutated GFP followed by a downstream truncated GFP. Transfection of I-SceI endonuclease induces double strand breaks in the upstream gene that can be repaired by the HR repair machinery leading to restored GFP expression that is quantified by fluorescence activated cell sorting (FACS). **B** U2OS cells were treated with 0 (DMSO) 5, 7, 10 μM of the LCKi PP2 for 48 h. Alternatively, cells were transfected with Sh Con, LCK KD1 or KD2 for 24 h and incubated in serum enriched medium for another 24 h. Cells were then subjected to DR-GFP assay followed by FACS. **C** Ovarian cancer cells were treated with PP2 or Olaparib for 48 h and immunoblot experiment was performed to check PARylation. **D** CP70 and SKOV3 cells were treated with 0 (DMSO) 5, 7, 10 μM of PP2 for 48 h then harvested, lysed, and immunoblotted for Ku70 and Ku80 protein expression. GAPDH was used as loading control. **E** Schematic model summarizing LCK inhibition specificity for HR DNA repair. One way ANOVA analysis was performed with Tukey's multiple comparisons test to compare different groups (* $p < 0.05$, ** $p < 0.01$, *** $p < 0.001$)

This indicates that LCK inhibition attenuates HR repair efficiency in cancer cells.

DNA damage leads to activation of several repair pathways including PARP, HR, and NHEJ [26]. As our studies indicated LCK inhibition attenuates HR repair proteins, we assessed LCK's impact on the expression of alternative DNA repair pathways, including PARP and NHEJ, in CP70 and SKOV3 cells. The LCK inhibitor PP2 did not inhibit PARylation in CP70 and SKOV3 cells (Fig. 4C). Ku70 and Ku80 proteins are a critical components of the NHEJ pathway [27]. After PP2 treatment, Ku80 protein expression was elevated in CP70, but not in SKOV3 (Fig. 4D). Ku70 protein expression was not changed in either CP70 or SKOV3 after PP2 exposure (Fig. 4D). In

parallel, Ku70 and Ku80 expression levels in CRL1978 cells did not change following PP2 treatment (Supplementary Fig. S10D). These findings indicate that LCK inhibition targets HR repair proteins independent of induction of NHEJ repair mechanisms (Fig. 4E).

LCK inhibition augments PARPi induced DNA damage and genomic instability

We performed single cell gel electrophoresis (alkaline COMET) assay to quantify the extent of double and single strand DNA breaks by visualizing tail area [28]. CP70 and SKOV3 cells were incubated with either PP2, olaparib, or both. Treated cells were processed and stained with SYBR Gold to detect and measure the tail moment (Fig. 5A). PP2 and olaparib alone displayed a comparable increase in comet tails compared to DMSO (Fig. 5B). The combination of PP2 and olaparib induced a fourfold increase in comet tail area compared to monotherapy (Fig. 5B).

PARP inhibitors have been reported to induce genomic instability, leading to chromosomal aberration and DNA damage in cancer cells [29, 30]. Chromosomal damage can be detected by chromosomal breaks, gaps, and radial formations. We identified multiple breaks, gaps, and radial formation in PP2 and olaparib-treated cells (Fig. 5C). PP2 and olaparib displayed a comparable increase in chromosomal damage when compared to DMSO (Fig. 5D). The combination of PP2 and olaparib displayed increased chromosomal damage in both CP70 and SKOV3 cells (Fig. 5D).

Based on this analysis, we assessed whether the LCK inhibitor PP2 could potentiate PARPi, olaparib, to augment the DNA damage response (Fig. 5E). Olaparib treatment led to an increase in BRCA1 expression and a detectable increase in γH2AX expression in SKOV3 cells (Fig. 5E). Co-treatment with PP2 was sufficient to suppress BRCA1 expression and significantly augment γH2AX expression in a dose-dependent manner (Fig. 5E). Our findings indicate LCK inhibition leads to HR deficiency. As proof of concept, we tested the impact of LCK silencing on the efficacy of olaparib in SKOV3 and CP70 cells via colony formation assay. Olaparib sensitivity was analyzed in parental (WT), KO, OE (Fig. 5F). We quantified colony formation and observed that IC_{50} value of Olaparib were as following: CP70 parental: 0.97 μM, CP70 LCK KO: 0.13 μM and CP70 LCK OE (In KO background): 1.34 μM. (Fig. 5F, Supplementary Fig. S12). We replicated these findings by silencing with shRNA in CP70 and SKOV3 cells (Supplementary Fig. S12A and B). shCon, KD1, and KD2 cells were treated with various concentrations of olaparib and plated for colony formation. In CP70 cells, silencing LCK inhibited colony formation with greater efficiency in olaparib-treated compared to shCon treated cells (Supplementary Fig. S12A, B). Similarly, in SKOV3 cells, the number of colonies were significantly decreased after olaparib treatment in KD1 and KD2 cells as compared to shCon cells (Supplementary Fig. S12C, D). These findings support the hypothesis that olaparib has a higher efficacy in LCK-deficient cancer cells and indicate that LCK inhibition is sufficient to sensitize eEOC to PARPi.

LCK inhibition potentiates therapeutic efficacy of PARPi in in vivo

To test whether LCK impacts olaparib efficacy in preclinical models of eEOC, we injected KO and OE CP70 cells into mice and once tumors were detected, we treated with 3 doses of Olaparib 50 mg/kg for 5 days (Fig. 6A). KO and OE CP70 exhibited nearly identical tumor growth in vehicle-treated mice (Fig. 6B and C). Olaparib treatment led to significant tumor suppression of in OE mice and to complete suppression of tumor growth in KO mice (Fig. 6B and C). These findings indicate that LCK inhibition potentiates olaparib synthetic lethality.

We next performed a molecular analysis of tumor sections from OE and KO cells treated without and with olaparib. TUNEL assay was used to detect apoptotic DNA fragmentation and indicated no positive cells (green fluorescence) in OE and KO tumors, indicating no apoptotic cells (Fig. 6D, Supplementary Fig. S13). Tumors from olaparib-treated mice exhibited few TUNEL-positive cells present in OE tumors, whereas most cells were TUNEL-positive in KO tumors. Next, tumors were assessed for presence of γH2AX in tissue sections by immunohistochemistry (Fig. 6E). Vehicle treated mice exhibited a low level of γH2AX in both KO and OE cohort (Fig. 6E). Tumors from olaparib-treated mice exhibited low levels of γH2AX expression in OE, whereas most cells were positive in KO group (Fig. 6E). These findings indicate multiple DNA double-strand breaks were generated due to suppression of LCK and inhibition of PARP. We next assayed for expression of CD31, an indicator of microvessel (angiogenesis) density and of tumor mass and growth. Vehicle treated mice exhibited high CD31 positive staining in both KO and OE cohort (Fig. 6F). Tumors from olaparib-treated mice exhibited high levels of CD31 expression in OE, whereas there was no detectable CD31 in the KO group (Fig. 6F). These findings suggested that olaparib was also sufficient to inhibit tumor angiogenesis, corroborating previous findings which showed that PARP facilitates tumor vascularization by augmenting CD31 and VEGF [31].

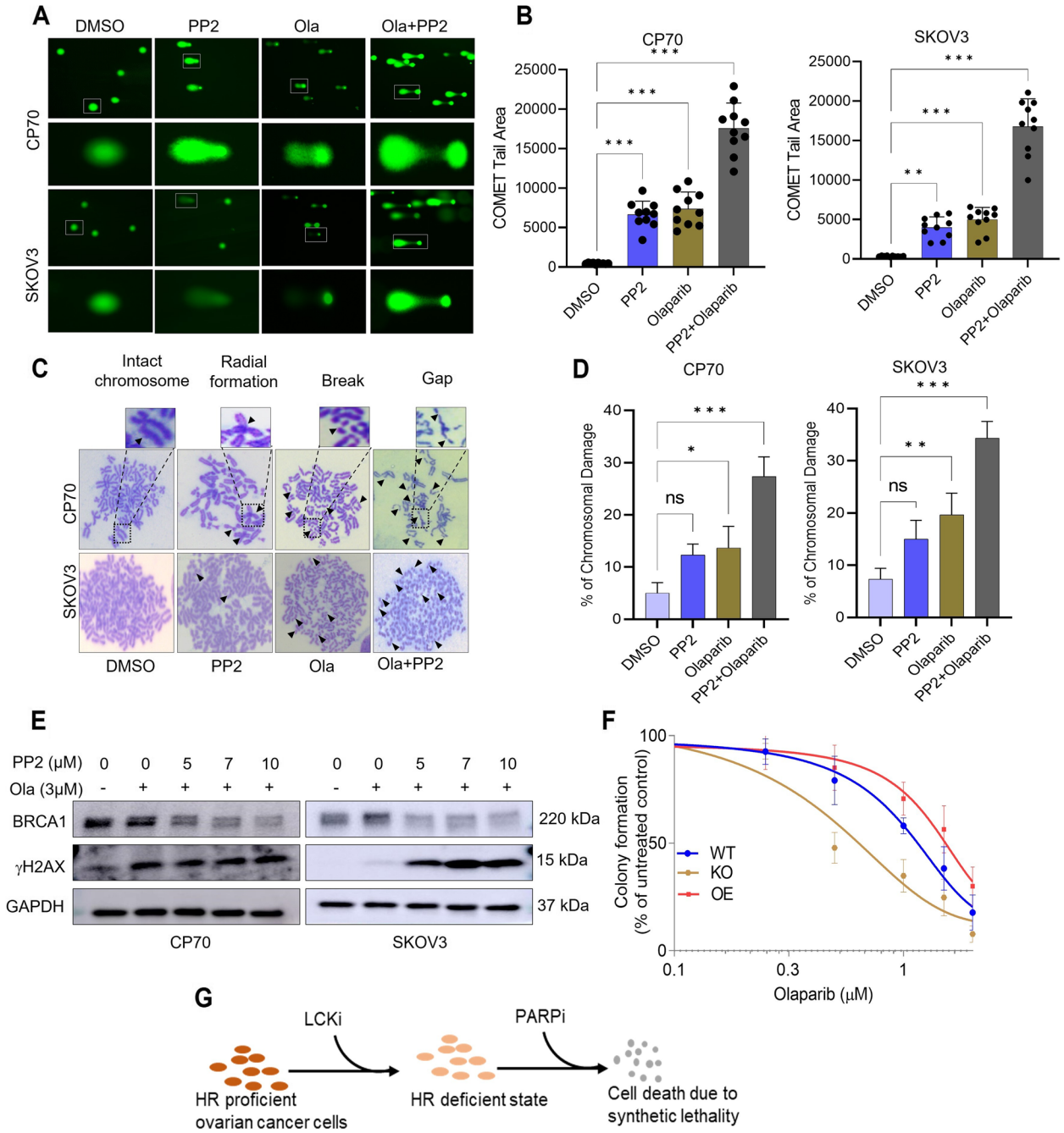

Fig. 5 LCKi promotes genomic instability and augments PARPi induced genomic instability in ovarian cancer cells. **A** Single cell electrophoresis or COMET assay was used to validate and independently quantify the observed DNA damage. CP70 and SKOV3 cells were treated with PP2 5 μM and/or Olaparib 3 μM for 48 h. Cells (1×10^5 Cells/ml) were then harvested and mixed with LMAgarose (1:10 V/V). 50μL of LMAgarose solution was spread on a COMET slide and subjected to single-cell gel electrophoresis. **B** Extent of DNA damage was estimated based on measurement of COMET tail area using Image J. **C** CP70 and SKOV3 cells treated with PP2 5 μM and/or Olaparib 3 μM for 48 h followed by chromosomal aberration assay analysis. Arrowheads indicate the presence of abnormalities in chromosomes including breaks, gaps, and radials. **D** Abnormities in chromosomes were quantified (Chromosomal break, gap, radial formation) by counting by visual observation. **E** CP70 and SKOV3 cells were treated with Olaparib and PP2 for 48 h. Cells were harvested, lysed, and blotted for BRCA1 and γH2AX. **F** CP70 Parental (WT), KO, and OE (in KO background) cells were treated with Olaparib in dose dependent manner for 12 days. To identify colonies, plates were stained with crystal violet and images were captured. Colonies formed were counted and plotted as percentage of control formation in the graph. **G** Schematic showing LCK inhibition was sufficient to induce HR deficient state and subsequent treatment with PARP inhibitor promoted cell death. One way ANOVA analysis was performed with Tukey's multiple comparisons test to compare different groups (* $p < 0.05$, ** $p < 0.01$, *** $p < 0.001$). Each experiment was repeated at least three times

Discussion

Endometrioid ovarian cancer, while rare, lacks effective therapeutic strategies and are HR proficient [32]. Our studies identified a strategy to induce HR deficiency in endometrioid ovarian cancer. The clinical relevance of LCK expression in EOC was previously evaluated by Kaplan–Meier analysis [18]. The data indicates that high levels of LCK expression is associated with worse clinical outcomes in endometrioid ovarian cancer and expression of LCK is increased in endometrioid ovarian cancer [33]. We determined that LCK complex formation with BRCA1 and RAD51 is induced response to DNA damage. We show that interaction of LCK with BRCA1 and RAD51 requires kinase activity or phosphorylation on Y394, indicating active LCK is necessary for complex formation [20]. LCK inhibition via genetic or pharmacologic disruption is sufficient to attenuate dsDNA damage repair and leads to synthetic lethality with PARPi. Our findings indicate that activation and catalytic activity of LCK is necessary for DNA damage repair. Previous studies indicate that kinase dead LCK remains in closed and inactive conformation [34]. Phosphorylation on Y394 results in stabilized and open structure leading to enhanced kinase activity and substrate binding [35, 36]. Our findings indicate the open and active form of LCK having intact kinase activity facilitates the interactions with RAD51 and BRCA1 proteins. In addition, we show that LCK stabilizes RAD51 and BRCA1 proteins. Collectively, kinase activity and autophosphorylation are necessary for functional DNA repair, as shown by γH2AX and RAD51 foci formation assays. These findings indicate that LCK kinase activity and autophosphorylation is essential for interaction with HR repair proteins BRCA1 and RAD51 during DNA damage response. Moreover, inhibition or disruption of the non-receptor tyrosine kinase LCK attenuates the expression of HR proteins RAD51, BRCA1, and BRCA2 in eEOC. This complements our previous study showing that LCK overexpression or LCK inhibition modulated the mRNA levels of HR DNA repair genes including *RAD51, BRCA1, and BRCA2* [17]. Here, we showed that LCK modulates HR genes at the protein level. This leads to functional consequences as the inhibition of LCK, via shRNA or pharmacologic inhibitor, leads to inhibition of DNA damage repair as assessed using the established DR-GFP assay in U2OS osteosarcoma cells. LCK does not impact PARP and NHEJ repairs, the alternate mechanisms for repair of double strand breaks by direct ligation independent of an homologous template [27]. Importantly, NHEJ repair proteins Ku70 and Ku80 expression levels were not impacted by PP2 treatment. Thus, LCK kinase activity is necessary for maintaining HR proficiency. Finally, we demonstrated that LCK disruption is sufficient to sensitize endometrioid ovarian cancer cells to olaparib. These findings are consistent with our data indicating that LCK inhibition leads to chemosensitization to cisplatin treatment in endometrioid ovarian cancer.

We determined for the first time that the LCK protein is upregulated in response to DNA damage in eEOC. DNA damage by etoposide, methyl methanesulfonate (MMS), and by UV radiation induces LCK protein expression. This is also corroborated by previous findings that indicate fractionated radiation induces stem cell populations in human gliomas to display LCK activation [37]. Phosphorylation of LCK (pY394) was elevated in etoposide, MMS, and UV-treated SKOV3 cells and in UV-treated CP70 cells as compared to untreated cells. We found that DNA damage led to nuclear localization of both total and pY394 LCK protein, a finding supported by immunofluorescence analysis of pY394 LCK following DNA damage. This finding is unprecedented as LCK is localized to the inner leaflet of the cell membrane on microdomains [38]. In support of our findings previous studies indicate that constitutively active LCK is found in the nucleus where it binds at the promoter region of LIM domain only 2 (LMO2) leading to gene expression [39]. Collectively, we show that LCK is activated by DNA damage, leading to nuclear translocation and subsequent activation of HR repair pathways.

The implications of LCK regulation of HR repair in response to DNA damage provides a therapeutic opportunity. We show that LCK inhibition potentiates the activity of PARPi to induce synthetic lethality. The simultaneous inhibition of LCK and PARP with pharmacological agents PP2 and olaparib shows significantly greater DNA damage and chromosomal aberration compared to

(See figure on next page.)

Fig. 6 Disruption of LCK leads to inhibition ovarian tumor treated with Olaparib (**A**) Schematic model of animal study. CP70 LCK KO and LCK OE cells were injected intraperitoneally in NSG mice. After 12 days, PARP inhibitor Olaparib i.p. (50 mg/kg) was administered 5 days/week. **B** After three weeks of Olaparib treatment, tumor volume was detected by IVIS imaging. **C** Tumor growth kinetics in tumor bearing mice injected with LCK KO and LCK OE CP70 cells. Mice were treated with vehicle or Olaparib. **D** TUNEL assay to detect DNA fragmentation in tumor tissue sections. TUNEL positive cells were counted from five images and plotted (Supplemental file S13 A). **E** IHC staining of γH2AX of tumor sections from different groups. γH2AX positive cells were counted from five images and plotted in graph (Supplemental file S13 B). **F** CD31 expression (Indicator of microvessel density and growth) of tumor sections from different group of mice. Microvessel density was counted from five images and plotted in graph (Supplemental file S13 C). Images are representative of two tumors from each cohort. We quantified the staining from 5 fields from each mouse. Images were captured at 20X magnification. One way ANOVA analysis was performed with Tukey's multiple comparisons test to compare different groups (* $p < 0.05$, ** $p < 0.01$, *** $p < 0.001$). Each experiment was repeated at least three times

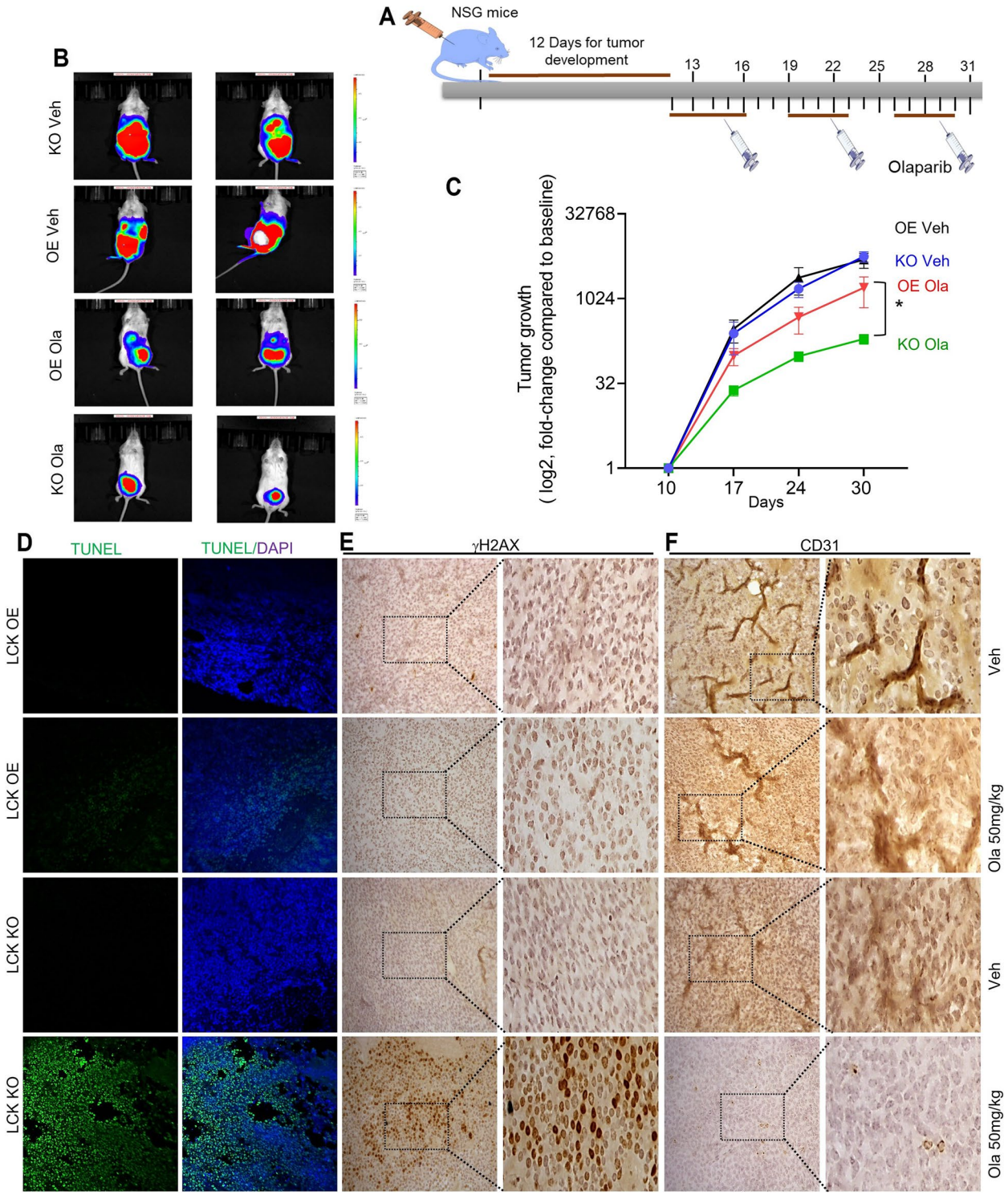

Fig. 6 (See legend on previous page.)

only either PP2 or olaparib treatment in eEOC cells. PP2 treatment is sufficient to attenuate DNA repair, augmenting the effect of olaparib in ovarian cancer cells. Finally, our in vivo studies showed that olaparib efficacy was enhanced in CP70 LCK KO compared to ovarian tumor bearing mice.

Our studies provides proof of concept for utility of LCK inhibitors to disrupt HR DNA damage repair.

Indeed, several strategies are currently being explored in the clinic to increase use of PARP targeted therapy in HR proficient cancers. CDK1 and CDK12 inhibition led to HR deficiency by decreasing HR repair proteins RAD51, BRCA1, and BRCA2 in lung cancer [9]. Further, inhibition of BET proteins also led to attenuation of RAD51 and BRCA1 proteins in breast, ovarian, and prostate cancer models [2]. PI3K inhibition is also sufficient to reduce BRCA1 and BRCA2 expression, hampering HR repair in triple-negative breast cancer [40]. Other reported targets are HSP90 [41] and VEGFR3 [42] shown to attenuate RAD51, BRCA1, and BRCA2 expressions in ovarian cancer. Concurrent inhibition of LCK enhanced the efficacy of PARPi in HR proficient cancer models in preclinical settings. Clinical trials are ongoing to assess the efficacy of PARPi in combination with CDK1/12 inhibitors, PI3K inhibitor, and VEGFR3 inhibitors [3]. Our findings complement these studies and identify an alternate signaling pathway for enhancing PARP targeted therapy in eEOC.

These findings provide an innovative new strategy for inducing an HR-deficient status in an otherwise HR-proficient tumor. We identify targeted therapies that compromise HR repair genes and augment sensitivity to PARPi. Our study defines the mechanistic impact of LCK and potentially other non-receptor tyrosine kinases in regulation of HR repair that is apparently crucial to ovarian cancer's response to chemotherapy and PARP inhibitors. This study highlights new clinical applications that target LCK, expanding PARPi utility. The studies provide support for future clinical studies using combination of LCK inhibitors with PARP inhibitors to improve patient outcomes.

Methods

Cell lines and culture conditions

Cisplatin resistant eEOC cancer cells CP70 were a gift from Analisa Difeo (University of Michigan) and SKOV3 were purchased from American Type Culture Collection (ATCC). CP70 and SKOV3 cells are endometrioid subtype of ovarian cancer. Both cells are cisplatin resistant and HR proficient. As expected, PARP inhibitors are not efficacious as the cells are HR proficient. We used these cell to demonstrate that inhibiting LCK would lead to reduced chemoresistance including sensitivity to PARPi. Others cell lines used in this study are mentioned in the resource table. Cells were grown in DMEM and McCoy's 5A media respectively, supplemented with 10% fetal bovine serum at 37 °C in humidified incubator in 5% CO2. Cells were tested and confirmed as mycoplasma contamination negative on a quarterly basis. Cells were passaged by treatment with trypsin/EDTA solution when they reached 80–90% confluence and further passaged or seeded for experiments.

Chemicals and reagents

We used several pharmacological agents in our study. The PARP inhibitor (Olaparib) [43], the LCK inhibitor (PP2) [23, 24] and the radiomimetic drug, etoposide [44] were purchased as shown in the resource table. Inhibitors were dissolved in 100% DMSO to make stock concentrations and kept at -20 °C until use. The details of chemical, reagents, primary antibodies, and secondary antibody details are outlined in the resource table (Supplementary Table S12).

Plasmid construct mutants

Myc-tagged LCK containing plasmid was generated using pENTR/D-TOPO cloning kit (Thermo Scientific) according to manufacturer instructions. Briefly, Myc-LCK gene block was purchased from Integrated DNA Technologies (IDT, USA). Myc-LCK was cloned into pENTR/D-TOPO vector. The entry clone was transferred into a destination vector, pLenti CMV Puro DEST (Addgene). The plasmid was validated by DNA sequencing (Eurofins). LCK mutants 192F, Y394F, 273R were generated by site directed mutagenesis and sequenced. Each mutant was cloned into a lenti viral vector, pLenti CMV Puro DEST (Addgene) for subsequent use.

Lentivirus production

Lentiviral particles for LCK silencing were generated using established lab protocols [17]. Briefly HEK293T cells were seeded into 6 well plates. The next day cells were transfected with pRSV-Rev, pMDLg/pRRE, pMD2.G and lentivral vector expressing shRNA for targeting LCK (KD1, TRCN0000426292, KD2, TRCN0000001599). Following 24 h incubation, transfection media was replaced with fresh DMEM medium. 48 h post transfection, lentiviral particle containing media was filtered to remove cell debris and added to CP70 and SKOV3 cells. Fresh media was subsequently added to the HEK-293 T transfection plates and incubated for an additional 24 h followed by filtration and addition to further CP70 and SKOV3 cells. Transduced CP70 and SKOV3 cells were identified using 1.5ug/ml and 2ug/ml puromycin (Thermo Scientific) selection respectively.

Generation of CRISPR/Cas9 KO cells

CP70 cells were used to generate LCK CRISPR/Cas9 knockout cells according to the manufacturer protocol (Santa Cruz Biotechnology). Briefly, cells were transfected with GFP labelled LCK CRISPR/Cas9 plasmid using lipofectamine 3000 (Thermo Scientific) in the presence of antibiotic-free, FBS-enriched, Optimem media. Following transfection, cells were kept in transfection medium for 24 h, then replaced with fresh culture media. After an additional 24 h, transfected cells

were screened for GFP expression using a flow cytometer, and the $GFP^{+/high}$ population was isolated and plated as single cells into a 96 well plate. Cells were grown and expanded in accordance with standard culture techniques as stated above, followed by western blotting for LCK protein expression with anti-LCK antibody (0.5 µg/mL, R & D Systems). Clones with the lowest LCK expression compared to parental cells were considered LCK KO cells.

Western blot analysis

Western blot analysis was performed as reported with modifications as follows [45, 46]. Briefly, cancer cells were washed with chilled Dulbecco's phosphate buffered saline (PBS) two times at the end of treatment. NP-40 lysis buffer (Invitrogen) was added dropwise to the plates and placed on ice for 10 min. The NP-40 lysis buffer contains 50 mM Tris, pH 7.4, 250 mM NaCl, 5 mM EDTA, 50 mM NaF, 1 mM Na3VO4, 1% Nonidet™ P40 (NP40), 0.02% NaN3 and was supplemented with 1 mM PMSF and 2 µg/ml protease cocktail inhibitor (PCI) (Sigma Aldrich). Cells were then collected in a 1.5 mL centrifuge tube by scraping, and incubated on ice for one hour with occasional vortexing. Lysates were centrifuged at 10,000 rpm for 10 min at 4 °C. Protein concentration was measured of each lysate supernatant by BCA kit analysis (Thermo Scientific). Protein samples were then prepared using 6×Laemmli dye containing BME (β-mercapto ethanol) and boiled for 5-10 min. Protein samples were subjected to SDS-PAGE gel electrophoresis using premade gradient gels (4–20%, Biorad). Proteins were transferred by wet transfer to a PVDF membrane (Millipore) at 4 °C overnight. Membranes were then blocked in 5% BSA in TBST for one hour at room temperature, and subsequently, incubated overnight at 4 °C in the following primary antibodies: T-LCK (1:1000 R&D Systems), T-LCK (1:1000 Proteintech), P-LCK 394 (1:1000 R&D Systems), RAD51 (1:1000, Proteintech), BRCA1 (1:500, EMD Millipore), BRCA2 (1:500, EMD Millipore), γH2AX (1:1000 Cell Signaling Technology), GAPDH (1:5000 Proteintech), and β-actin (1:4000 Proteintech). After primary antibody incubation membranes were washed three times with TBST (Tris-buffered saline containing 0.1% tween 20) washing buffer on a platform shaker. Membranes were incubated with HRP-conjugated rabbit (1:25000) or mouse (1:25000) secondary antibodies for one hour at room temperature, followed by three washes with TBST buffer. Chemiluminescence reagent (PerkinElmer) was added to detect immobilized proteins in PVDF membranes utilizing the ChemiDoc imaging system. Densitometry was performed using Image J software.

Nuclear protein isolation and co-immunoprecipitation analysis

CP70 and SKOV3 cells transduced with Myc-tagged LCK were treated with etoposide (10 µM) or DMSO for 24 h followed by replacement with fresh serum-enriched media for an additional 24 h. Cells were collected and washed with cold PBS two times, scraped and centrifuged. Cell pellets were then lysed with cytoplasmic and nuclear extraction buffers according to manufacturer protocols (NE-PER Nuclear and Cytoplasmic Extraction Kit, Thermo Scientific). Protein concentrations of nuclear lysates were estimated using the BCA method outlined above. For co-immunoprecipitation, nuclear protein lysates were incubated with 3 µg anti-Myc antibody (Proteintech) or 3 µg control antibody (Cell Signaling Technology) overnight at 4 °C with gentle rocking. Pre-cleaned protein A/G agarose beads (Thermo Scientific) were added to the lysates and incubated for 4 h at 4 °C on a rotating mixer. Beads were then collected by centrifugation and washed three times with chilled NP-40 lysis buffer. 6×Laemmli buffer (Alfa Aesar) containing BME was added and beads were boiled for 5 min. Samples were separated on SDS-PAGE and processed for western blot analysis as outlined above. Further, LCK overexpression (OE) SKOV3 (without Myc tagged) cells were treated with etoposide (10 µM) for 24 h. Then, serum-enriched media was added to replace drug-containing media and kept for another 24 h. Then, cells were collected, and nuclear lysates were prepared. Further immunoprecipitation/co-immunoprecipitation was performed after RAD51 pulled down as described above.

Gene conversion assay

Gene conversion assay or DR-GFP assay was performed according to reported methods [47]. Human osteosarcoma U2OS cells stably transfected with DR-GFP plasmid and I-SceI endonuclease expression vector pCBASce were kindly provided by Maria Jasin at Memorial Sloan-Kettering Cancer Center. Cells were treated with, PP2 (5, 7, and 10 µM) or DMSO vehicle for 48 h. Cells were then transfected with I-SceI endonuclease expression vector pCBASce using Lipofectamine 3000. In a separate set of experiments, U2OS cells with DR-GFP integration were transfected with shCon, LCK KD1 or KD2 for 24 h and incubated in serum enriched medium for another 24 h. Cells were further transfected with I-SceI plasmid for 24 h followed by incubation with serum enriched medium for 24 h. Live cells (Live/Dead dye kit, Thermo Scientific) were analyzed with a flow cytometer to estimate the percentage of GFP-positive cells.

Cell cycle analysis

Cells were grown in 60 mm Petri dish until they reached 70% confluency. Cells were then detached with trypsin treatment, harvested by centrifugation, and washed with PBS. Subsequently, cells were fixed in 70% chilled ethanol, stained with propidium iodide, washed with PBS, and analyzed by flow cytometry analysis. Samples were analyzed for DNA content to determine percentage of cells in G0/G1, S, and G2/M cell cycle phase. Each experiment was replicated three times and percentages of cell population was plotted by Graph pad prism software.

RAD51 and γH2AX nuclei staining and analysis

Laser scanning confocal microscopy was performed to detect RAD51 and γH2AX foci in cancer cells. Briefly, ovarian cancer cell, CP70 were grown on coverslips and treated with 10 μM etoposide or vehicle for 24 h followed by an additional 24 h in drug-free media. Coverslips were washed with PBS and fixed with 4% paraformaldehyde (Electron Microscopy Sciences) in PBS. Cells were permeabilized with 0.01% triton-X 100 (Fisher Scientific) for 5 min followed by a wash with chilled PBS and blocked with 3% goat serum (Thermo Scientific) for 1 h at room temperature. Cells were incubated with anti-RAD51 (1:250, Abcam) or anti-γH2AX (1:300, Cell Signaling Technology) antibodies overnight at 4 °C in a humidified chamber. Next, cover slips were washed 3X with PBS. Alexa fluorescent conjugated secondary antibodies were added to the coverslips and incubated for 1 h. Coverslips were washed 3×and mounted with DAPI containing Vectashield (Vector Lab). Images were captured by confocal microscope at 63×magnification in oil emersion (Leica SP8 confocal microscope). RAD51 and γH2AX foci were counted on 100 representative cells by image J software.

Metaphase spread analysis

Metaphase spread analysis was performed on LCKi and PARPi treated cells using established methods [30]. Briefly, cells were treated with LCK inhibitor, PP2 (5 μM) (Selleck Chemicals) and PARP inhibitor, olaparib (3 μM) (Selleck Chemicals) for 48 h. After treatment, cells were harvested. Cells were treated with colcemid (50 ng/ml) (Sigma) for 1.5 h then washed with PBS and placed in 0.075 mol/L KCl (Sigma) solution for 20 min. Subsequently, cells were washed with PBS and fixed in carnoy fixative solution (Methanol: acetic acid 3:1) added dropwise followed by one hour incubation. Cell pellets were collected, and fixative solution was added and incubated at 4 °C for 24 h. Cell pellets were collected and small amount fixative solution was added and cell suspension was slowly dropped on glass slides and allowed to dry at 37 °C. Slides were then stained with Giemsa solution (Sigma Aldrich). Images were captured at 100X magnification with a bright field microscope. Abnormalities in chromosomes were quantified (Chromosomal break, gap, radial formation) by visually counting five nuclei per treatment group. Percent of damage was calculated as number of chromosomal damages/5*100.

Single cell electrophoresis assay

Single cell electrophoresis assay or comet assay was performed according to a previously reported method [48]. This experiment was performed following the manufacturer's instructions (Trevigen). Briefly, CP70 and SKOV3 eEOC cells were treated with 5 μM PP2 and/or 3 μM Olaparib for 48 h. Comet LMAgarose was melted at 90 °C for 10 min in a water bath then cooled for 20 min to 37 °C. Treated cells were detached from plates using trypsin. Serum enriched media was added to neutralize the trypsin. Cell suspension was washed twice with chilled 1X Ca^{++} and Mg^{++} free PBS, and subsequently suspended at 1 X 10^5 cells/ml in chilled 1X PBS buffer (Free of Ca++and Mg++). For the alkaline comet assay, the cell suspension was mixed with molten LMAgarose at 37 °C. Immediately, 50μL LMAgarose mix was spread on glass microscope slides and incubated at 4 °C for 30 min in the dark. Slides were incubated in lysis solution (provided in kit) overnight at 4 °C. The next day comet slides were incubated in alkaline unwinding solution at room temperature for 20 min. Agarose gel electrophoresis (21 V for 30 min) was performed using alkaline electrophoresis protocol. After electrophoresis, slides were briefly immersed in distilled water twice and then immersed in 70% ethyl alcohol for 5 min. Slides were dried and 100 μl of SYBR gold (excitation/emission is 496 nm/522 nm) was added on agarose and kept for 30 min in the dark. Slides were washed with water, dried, and visualized by fluorescence microscopy. Comet tail area was measured by the Image J software and ten comets were estimated and plotted in the graph. Percent of damage was calculated as number of chromosomal damages/10*100.

Colony formation assay

The pharmacological effect of olaparib in cancer cells was investigated by colony formation assay according to the earlier reported method [30]. Briefly, ovarian cancer cells CP70 and SKOV3 cells (WT, sh, LCK OE, LCK KO, LCK KD and mutants) were placed on 12 well plates. The next day, cells were treated with olaparib in a dose dependent manner for 12 days. During this time the media was changed every day using fresh drug. At the end of experiment, PBS was added to the well to wash the colony. Then, cells were fixed with 4% paraformaldehyde solution for 10 min. Cells were then washed two times with PBS

and incubated in 0.2% crystal violet solution for one hour at room temperature. After incubation cells were washed three times with PBS. Then, the images of six well plates were captured and number of colony forming area was analyzed by Image J software.

Cell titer glo viability assay

CP70 (WT, OE, KD, KO and LCK mutants, Y394F, K273R and Y192F) cells were collected after trypsinization. Cells were counted and 4000 cells were plated in each well of a 96 well plate. Cells were then treated with etoposide for 48 h in a dose dependent manner. Control cells were treated with vehicle (DMSO). After the drug treatment, Cell TiterGlo® Luminescent Cell viability assay reagent (Promega) mixture was prepared and added to the cells to lyse them for 10 min shaking and luminescence was measured via luminometer. Cell viability percentage was calculated as luminescence of treated group/luminescence of vehicle treated group × 100.

NHEJ gene expression

To check for NHEJ expression, CP70 and SKOV3 cells were grown on 60 mm petri dishes until 70% confluent. Cells were then treated with PP2 in a dose dependent manner (5, 7 and 10 μM) for 48 h and collected by scraping and Western blot was performed to assess protein expression of NHEJ markers Ku70 and Ku80.

In vivo animal study in NSG mice

In vivo antitumor efficacy of Olaparib was tested in NSG (NOD severe combined immunodeficient (SCID) IL2R gamma) mice. This study was approved (IACUC Protocol# 2707) by Institutional Animal Care and Use Committee (IACUC), Cleveland Clinic Lerner Research Institute. Animals were procured from BRU (Biological Response Unit) facility of the Cleveland Clinic. All cells used in this study were transfected (Lentiviral transfection) with pCDH-EF1a-eFFly-mCherry plasmid. Mice were injected with CP70 LCK knockout cells or CP70 LCK overexpression cells intraperitoneally (Cells: 0.5×10^6). After that mice were divided into four groups-**1**. Mice: CP70 LCK KO: Vehicle ($n = 8$), **2**. Mice: CP70 LCK KO: Olaparib (50 mg/kg) ($n = 8$), **3**. Mice: CP70 LCK OE: Vehicle (n = 8), **4.** Mice: CP70 LCK KO: Olaparib (50 mg/kg) ($n = 8$). Olaparib was dissolved in ddH_2O containing 4% DMSO and 30% polyethelene glycol (PEG300) and injected intraperitoneally. Animals were treated with olaparib for 5 days/week. Bioluminescence of the tumor were measured by in vivo imaging system (IVIS Spectrum CT, PerkinElmer). At the end of the experiment, mice were sacrificed according to the protocol of Institutional Animal Care and Use Committee (IACUC), Cleveland Clinic Lerner Research Institute. Tumor tissues were collected and preserved in 10% formalin solution.

Immunohistochemistry and TUNEL assay

Immunohistochemical (IHC) analysis and TUNEL assay of tumor sections were performed according to the earlier reported method [49]. Formalin fixed tissues were sent to histology core to make thin slice (around 5micron) of tissue embedded on glass slides. Next, slides were dipped in HistoClear to deparaffinize. Then sections were rehydrated in gradient ethanol (100%, 95%, 80% and 60% ethanol 5 min for each bath). For antigen retrieval, sections were put in Tris–EDTA buffer (pH9) and boiled in a pressure cooker for 10minand cooled for an hour. Slides were then blocked in 0.1% triton X-100 solution for 10 min to permeabilize, washed with PBS three times, blocked in 5% goat serum and 0.1% triton X-100 in 1X TBST at room temperature for one hour. Antibodies were added to the tissues and incubated for overnight at 4 °C. Next day, sections were washed three times with PBS followed by incubation with diluted Peroxidase Labeled Polymer for 30 min at room temperature.Sections were washed three times with PBS and diluted DAB chromogen was added to the tissue and incubated for 2-5 min until desired color was generated. Sections were washed three times and then hematoxylin staining was performed. After washing with PBS, tissue sections were dried and mounted with Cytoseal. Images were captured using upright microscope at 20 × magnification.

For TUNEL assay, tissue sections were processed for antigen retrieval and permeabilization as discussed earlier. Sections were washed three times with PBS. Then enzyme solution was prepared according to the manufacturer instructions. Slides were incubated in the enzyme for 60 min at 37 °C. Sections were washed three times with PBS and mounted with Vectashield containing DAPI.

Software and statistics

Graph pad prism software was utilized for graph preparation and to determine statistical significance (detailed in each figure legend). Image J was used for quantification of data. Experiment was performed with at least three replicates and repeated three times. p-value less than 0.05 was considered significant.

Abbreviations

eEOC	Endometrioid epithelial ovarian cancer
HR	Homologous recombination
LCK	Lymphocyte-specific protein tyrosine kinase
PARP	Poly(ADP-ribose) polymerase
DDR	DNA damage response
NHEJ	Non–homologous end joining

Supplementary Information

The online version contains supplementary material available at https://doi.org/10.1186/s13048-023-01194-2.

Additional file 1: Supplementary Fig. S1. Transfection efficiency of Myc tagged LCK in SKOV3 and CP70. SKOV3 and CP70 cells were transduced with EV or Myc tagged LCK plasmid by using lentiviral particle. Then, cells were checked for Myc and LCK expression. **Supplementary Fig. S2.** CP70 EV and CP70 LCK OE cells were treated with cycloheximide in a time dependent manner. Then, immunoblot analysis was performed to evaluate the expression of RAD51 and BRCA1 proteins (Main Fig. 1G, H). Half-lives were determined from digitized images. **Supplementary Fig. S3.** (A) CP70 WT, LCK KO (CRISPR/Cas9) and LCK OE (In CRISPR background) cells were treated with DMSO/etoposide 10μM for 24h. Then cells were kept in drug free media for another 24h. Then immunofluorescence study was performed to visualize γH2AX foci formation in different groups. (B) CP70 WT, LCK KO (CRISPR/Cas9) and LCK OE (In CRISPR background) cells were treated with DMSO/etoposide 10μM for 24h. Cells were put in drug free media for another 24h. Then immunofluorescence study was performed to visualize RAD51 foci formation in different groups. **Supplementary Fig. S4**. (A) CP70 cells (LCK OE, LCK Y394F, LCK K273R, and LCK Y192F, all constructs were introduced into the CP70 LCK KO cells) were treated with etoposide for 24h**.** Cells were then kept in drug free media for 24h. Immunofluorescence study was performed to visualize γH2AX foci formation. (B) CP70 cells (LCK OE, LCK Y394F, LCK K273R, and LCK Y192F) were treated with etoposide for 24h**.** Cells were then kept in drug free media for 24h. Immunofluorescence study was performed to visualize RAD51 foci formation. **Supplementary Fig. S5.** CP70 cells (LCK, LCK Y394F, LCK K273R, and LCK Y192F in LCK knock out background) were grown on cover slips and treated with etoposide for 24h followed by incubation for 0, 2, 4, 8 and 24h. Cells were then subjected to immunofluorescence analysis to visualize H2AX foci formation. **Supplementary Fig. S6**. (A) SKOV3 cells were treated with etoposide, and MMS for 24. After that cells were put in 24h in drug free media. Cells were then subjected to western blot analysis for checking protein expression. (B) DNA damage by UV radiation upregulates LCK phosphorylation. CP70 cells were treated with UV radiation for 1min, 2min and 4min. Cells were kept in serum enriched media for 24h. Then cells were subjected to western blot analysis to check the expression of P-LCK, T-LCK and BRCA1 expression. (C) SKOV3 LCK OE cells were treated with etoposide for 24h. Cells were then put in drug free media for another 24h. Cells were collected, and cytoplasmic and nuclear proteins were extracted for western blot analysis. **Supplementary Fig. S7.** (A, B) Protein quantification of T-LCK, BRCA1, and γH2AX in CP70 cells treated with etoposide and MMS (Main Fig. 3A). (C) Quantification of P-LCK and T-LCK in CP70 LCK OE cells treated with etoposide (Main Fig. 3B). (D) Quantification of BRCA1 protein in CP70 shCon, LCK KD1 and LCK KD2 cells treated with/without etoposide (Main Fig. 3E). (E) Quantification of BRCA1 protein expression in CP70 WT and LCK KO cells treated with/without etoposide (Main Fig. 3F). One way ANOVA analysis was performed with Tukey's multiple comparisons test to compare different groups (* $p < 0.05$, ** $p < 0.01$, *** $p < 0.001$). **Supplementary Fig. S8**. LCK modulates expression of HR repair proteins. (A) Western blot of CP70 and SKOV3 cells containing various lentiviral EV, LCK KD, KO, and OE to determine effects on LCK, BRCA1, BRCA2 and RAD51 expression. We detected a significant basal level of LCK in WT cells. In EV-OE panel, we used empty vector and LCK OE plasmid transduced in LCK knock out cells. (B) Western blot analysis of CP70 and SKOV3 LCK OE cells treated with PP2 in a dose dependent manner for 48hrs, demonstrating the effects of a pharmacological inhibitor of LCK on P-LCK, T-LCK, BRCA1, BRCA2, RAD51 and γH2AX protein expression. **Supplementary Fig. S9**. Cell cycle analysis by flow cytometry. (A) CP70 cells (LCK OE and KO) were grown to 70% confluency. Cells were harvested by trypsinization and fixed with chilled ethanol. Cell were then stained with propidium iodide and subjected to flow cytometry. Experiments were replicated three times. (B) Percentage of cell population in each phase of cell cycle are presented. One way ANOVA analysis was performed with Tukey's multiple comparisons test to compare different groups (* $p < 0.05$, ** $p < 0.01$, *** $p < 0.001$). **Supplementary Fig. S10**. (A) Pharmacological inhibition of LCK attenuates HR repair proteins in ovarian cancer cells. CP70, SKOV3 and CRL1978 cells were treated with the LCKi, PP2 for 48h. Cells were harvested, lysed, and analyzed by immunoblot to assess protein expression of BRCA1, BRCA2, RAD51, and γH2AX. (B) Western blot analysis in different cells to check the expression of LCK and BRCA1. U2OS is osteosarcoma cell line which was used in DR GFP assay. U2OS and U2OS: DR-GFP cells were examined for checking LCK and BRCA1 expression. These cells were also found to express LCK and BRCA1 like CP70 and SKOV3 cells. (C) Representative image of flow cytometry from DRGFP assay. Upper panel is shows GFP population of U2OS cells treated with PP2 and lower panel is shows GFP population in Sh Control, LCK KD1 and KD2 groups of U2OS cells. (D) CRL1978 cells were treated with increasing concentrations of PP2 for 48h and cells were harvested, lysed, and immunoblotted for Ku70, and Ku80 protein expression. GAPDH was used as loading control. **Supplementary Fig. S11**. (A) CP70 Parental cells and CP70 LCK KO and CP70 CD55 OE (In KO background) cells were treated with Olaparib in dose dependent manner for 12 days. After that colonies were stained with crystal violet and images were captured. (B) Number of Colony formation was counted and plotted as percentage of colony formation in the graph (Main fig 6G). IC50 values were shown in the table. **Supplementary Fig. S12**. (A, B) CP70 Sh Con or LCK knock down cells were treated with Olaparib in a dose dependent manner for 12 days. Number of colonies was counted and plotted using graph pad prism. (C, D) SKOV3 Sh Con or LCK knock down cells were treated with Olaparib in dose dependent manner for 12 days. Number of Colony formation was counted and plotted in the graph. **Supplementary Fig. S13**. (A) TUNEL assay to detect DNA fragmentation in tumor tissue sections. TUNEL positive cells were counted from five images and plotted in graph (Main fig. 8D). (B) IHC staining of γH2AX of tumor sections from different groups. γH2AX positive cells were counted from five images and plotted in graph (Main fig. 8E). (C) CD31 expression (Indicator of microvessel density and growth) of tumor sections from different group of mice. Microvessel density was counted from five images and plotted in graph (Main fig. 8F). Images are representative of two tumors from each cohort. We quantified the staining from 5 fields from each mouse. Images were captured at 20X magnification. One way ANOVA analysis was performed with Tukey's multiple comparisons test to compare different groups (* $p < 0.05$, ** $p < 0.01$, *** $p < 0.001$).

Acknowledgements

Authors thank the members of Reizes and Lathia Laboratories for helping to improve the scientific quality of the manuscript. We would like to thank Alex Myers for extensive editing the manuscript. We would like to thanks Dr. Debjit Khan from Fox Laboratory for insights on complex formation assays. We thank Dr. Gauravi Deshpande and the Lerner Research Imaging Core for helping in image acquisition by confocal microscopy, Amy Graham and Eric Schultz for flow cytometry, and we would also like to thank Dr. Suparna Mazumdar (Cleveland Clinic) for giving constructive comments of this study. Research in the Reizes laboratory is funded by Center of Research Excellence in Gynecologic Cancer from the Cleveland Clinic Foundation, VeloSano Bike to Cure, and the Laura J. Fogarty Endowed Chair for Uterine Cancer Research. Dr. Gong is supported by and NIH/NCI grant (R01 CA222195).

Authors' contributions

OR: Conceptualization, funding acquisition, reviewing the data, writing and editing the manuscript, and approval of final manuscript draft, GD: Data generation, design of experiment and writing the manuscript, RB: Data generation, design of experiment and writing the manuscript, CB: Generation of LCK mutants, RA: Generation of LCK construct, EE: Manuscript editing and formal analysis, KCT: Manuscript editing and formal analysis, KMC: LCK construct generation and formal review, AJP: Immunohistochemistry analysis, PGR: Manuscript editing and formal analysis, JL: Manuscript editing and formal analysis, ZG: Providing insight in various experiments and DR-GFP construct, reagents. GD and RB have contributed equally to this work. The author(s) read and approved the final manuscript.

Availability of data and materials

Data generated by the authors are included within the text and supplementary files or will be made available upon request to the corresponding author. Other reagents can be available upon request to the corresponding author.

Declarations

Competing interests

Ofer Reizes is an Associate Editor of Journal of Ovarian Research. All decisions on this manuscript were made by another senior editor. (The author(s) declare that they have no other competing interests.)

Author details

[1]Department of Cardiovascular and Metabolic Sciences, Lerner Research Institute, Cleveland Clinic Foundation, 9500 Euclid Avenue, Cleveland, OH 44195, USA. [2]Division of Gynecologic Cancer, Women's Health Institute, Cleveland Clinic, Cleveland, OH, USA. [3]Case Comprehensive Cancer Center, Cleveland, OH, USA. [4]Pathology and Lab Medicine, Cleveland Clinic, Cleveland, OH, USA. [5]Cancer Biology, Lerner Research Institute, Cleveland Clinic, Cleveland, OH, USA.

Received: 24 January 2023 Accepted: 24 May 2023
Published online: 27 June 2023

References

1. Siegel RL, Miller KD, Wagle NS, Jemal A. Cancer statistics, 2023. CA Cancer J Clin. 2023;73:17–48.
2. Yang L, Zhang Y, Shan W, Hu Z, Yuan J, Pi J, et al. Repression of BET activity sensitizes homologous recombination-proficient cancers to PARP inhibition. Sci Transl Med. 2017;9(400):eaal1645.
3. Konstantinopoulos PA, Ceccaldi R, Shapiro GI, D'Andrea AD. Homologous Recombination Deficiency: Exploiting the Fundamental Vulnerability of Ovarian Cancer. Cancer Discov. 2015;5:1137–54.
4. O'Connor MJ. Targeting the DNA Damage Response in Cancer. Mol Cell. 2015;60:547–60.
5. Moore K, Colombo N, Scambia G, Kim BG, Oaknin A, Friedlander M, et al. Maintenance Olaparib in Patients with Newly Diagnosed Advanced Ovarian Cancer. N Engl J Med. 2018;379:2495–505.
6. Creeden JF, Nanavaty NS, Einloth KR, Gillman CE, Stanbery L, Hamouda DM, et al. Homologous recombination proficiency in ovarian and breast cancer patients. BMC Cancer. 2021;21:1154.
7. Galluzzi L, Senovilla L, Vitale I, Michels J, Martins I, Kepp O, et al. Molecular mechanisms of cisplatin resistance. Oncogene. 2012;31:1869–83.
8. Tumiati M, Hietanen S, Hynninen J, Pietila E, Farkkila A, Kaipio K, et al. A Functional Homologous Recombination Assay Predicts Primary Chemotherapy Response and Long-Term Survival in Ovarian Cancer Patients. Clin Cancer Res. 2018;24:4482–93.
9. Johnson N, Li YC, Walton ZE, Cheng KA, Li D, Rodig SJ, et al. Compromised CDK1 activity sensitizes BRCA-proficient cancers to PARP inhibition. Nat Med. 2011;17:875–82.
10. Alagpulinsa DA, Ayyadevara S, Yaccoby S, Shmookler Reis RJ. A Cyclin-Dependent Kinase Inhibitor, Dinaciclib, Impairs Homologous Recombination and Sensitizes Multiple Myeloma Cells to PARP Inhibition. Mol Cancer Ther. 2016;15:241–50.
11. Abbotts R, Topper MJ, Biondi C, Fontaine D, Goswami R, Stojanovic L, et al. DNA methyltransferase inhibitors induce a BRCAness phenotype that sensitizes NSCLC to PARP inhibitor and ionizing radiation. Proc Natl Acad Sci U S A. 2019;116:22609–18.
12. Prakash R, Zhang Y, Feng W, Jasin M. Homologous recombination and human health: the roles of BRCA1, BRCA2, and associated proteins. Cold Spring Harb Perspect Biol. 2015;7:a016600.
13. Johnson SF, Cruz C, Greifenberg AK, Dust S, Stover DG, Chi D, et al. CDK12 Inhibition Reverses De Novo and Acquired PARP Inhibitor Resistance in BRCA Wild-Type and Mutated Models of Triple-Negative Breast Cancer. Cell Rep. 2016;17:2367–81.
14. Meinhold-Heerlein I, Fotopoulou C, Harter P, Kurzeder C, Mustea A, Wimberger P, et al. The new WHO classification of ovarian, fallopian tube, and primary peritoneal cancer and its clinical implications. Arch Gynecol Obstet. 2016;293:695–700.
15. Winterhoff B, Hamidi H, Wang C, Kalli KR, Fridley BL, Dering J, et al. Molecular classification of high grade endometrioid and clear cell ovarian cancer using TCGA gene expression signatures. Gynecol Oncol. 2016;141:95–100.
16. Ren T, Sun TT, Wang S, Sun J, Xiang Y, Shen K, et al. Clinical analysis of chemo-resistance risk factors in endometriosis associated ovarian cancer. J Ovarian Res. 2018;11:40.
17. Saygin C, Wiechert A, Rao VS, Alluri R, Connor E, Thiagarajan PS, et al. CD55 regulates self-renewal and cisplatin resistance in endometrioid tumors. J Exp Med. 2017;214:2715–32.
18. Crean-Tate KK, Braley C, Dey G, Esakov E, Saygin C, Trestan A, et al. Pretreatment with LCK inhibitors chemosensitizes cisplatin-resistant endometrioid ovarian tumors. J Ovarian Res. 2021;14:55.
19. Yu PN, Yan MD, Lai HC, Huang RL, Chou YC, Lin WC, et al. Downregulation of miR-29 contributes to cisplatin resistance of ovarian cancer cells. Int J Cancer. 2014;134:542–51.
20. Liaunardy-Jopeace A, Murton BL, Mahesh M, Chin JW, James JR. Encoding optical control in LCK kinase to quantitatively investigate its activity in live cells. Nat Struct Mol Biol. 2017;24:1155–63.
21. Kastle M, Merten C, Hartig R, Kaehne T, Liaunardy-Jopeace A, Woessner NM, et al. Tyrosine 192 within the SH2 domain of the Src-protein tyrosine kinase p56(Lck) regulates T-cell activation independently of Lck/CD45 interactions. Cell Commun Signal. 2020;18:183.
22. Zhu S, Paydar M, Wang F, Li Y, Wang L, Barrette B, et al. Kinesin Kif2C in regulation of DNA double strand break dynamics and repair. Elife. 2020;99:e53402.
23. Zhu X, Kim JL, Newcomb JR, Rose PE, Stover DR, Toledo LM, et al. Structural analysis of the lymphocyte-specific kinase Lck in complex with non-selective and Src family selective kinase inhibitors. Structure. 1999;7:651–61.
24. Nyakeriga AM, Garg H, Joshi A. TCR-induced T cell activation leads to simultaneous phosphorylation at Y505 and Y394 of p56(lck) residues. Cytometry A. 2012;81:797–805.
25. Nakanishi K, Cavallo F, Brunet E, Jasin M. Homologous recombination assay for interstrand cross-link repair. Methods Mol Biol. 2011;745:283–91.
26. Scully R, Panday A, Elango R, Willis NA. DNA double-strand break repair-pathway choice in somatic mammalian cells. Nat Rev Mol Cell Biol. 2019;20:698–714.
27. Chang HHY, Pannunzio NR, Adachi N, Lieber MR. Non-homologous DNA end joining and alternative pathways to double-strand break repair. Nat Rev Mol Cell Biol. 2017;18:495–506.
28. Xiao M, Guo J, Xie L, Yang C, Gong L, Wang Z, et al. Let-7e Suppresses DNA Damage Repair and Sensitizes Ovarian Cancer to Cisplatin through Targeting PARP1. Mol Cancer Res. 2020;18:436–47.
29. Lloyd RL, Wijnhoven PWG, Ramos-Montoya A, Wilson Z, Illuzzi G, Falenta K, et al. Combined PARP and ATR inhibition potentiates genome instability and cell death in ATM-deficient cancer cells. Oncogene. 2020;39:4869–83.
30. Kim H, George E, Ragland R, Rafail S, Zhang R, Krepler C, et al. Targeting the ATR/CHK1 Axis with PARP Inhibition Results in Tumor Regression in BRCA-Mutant Ovarian Cancer Models. Clin Cancer Res. 2017;23:3097–108.
31. Yasukawa M, Fujihara H, Fujimori H, Kawaguchi K, Yamada H, Nakayama R, et al. Synergetic Effects of PARP Inhibitor AZD2281 and Cisplatin in Oral Squamous Cell Carcinoma in Vitro and in Vivo. Int J Mol Sci. 2016;17:272.
32. da Cunha Colombo Bonadio RR, Fogace RN, Fogace RN, Miranda VC, Diz M. Homologous recombination deficiency in ovarian cancer: a review of its epidemiology and management. Clinics (Sao Paulo). 2018;73:e450s.
33. Tothill RW, Tinker AV, George J, Brown R, Fox SB, Lade S, et al. Novel molecular subtypes of serous and endometrioid ovarian cancer linked to clinical outcome. Clin Cancer Res. 2008;14:5198–208.
34. Bommhardt U, Schraven B, Simeoni L. Beyond TCR Signaling: Emerging Functions of Lck in Cancer and Immunotherapy. Int J Mol Sci. 2019;20(14):3500.
35. Salmond RJ, Filby A, Qureshi I, Caserta S, Zamoyska R. T-cell receptor proximal signaling via the Src-family kinases, Lck and Fyn, influences T-cell activation, differentiation, and tolerance. Immunol Rev. 2009;228:9–22.
36. Wei QR, Brzostek J, Sankaran S, Casas J, Hew LSQ, Yap JW, et al. Lck bound to coreceptor is less active than free Lck. P Natl Acad Sci USA. 2020;117:15809–17.
37. Kim RK, Yoon CH, Hyun KH, Lee H, An S, Park MJ, et al. Role of lymphocyte-specific protein tyrosine kinase (LCK) in the expansion of glioma-initiating cells by fractionated radiation. Biochem Biophys Res Commun. 2010;402:631–6.

38. Bijlmakers MJ, Marsh M. Trafficking of an acylated cytosolic protein: newly synthesized p56(lck) travels to the plasma membrane via the exocytic pathway. J Cell Biol. 1999;145:457–68.
39. Venkitachalam S, Chueh FY, Yu CL. Nuclear localization of lymphocyte-specific protein tyrosine kinase (Lck) and its role in regulating LIM domain only 2 (Lmo2) gene. Biochem Biophys Res Commun. 2012;417:1058–62.
40. Ibrahim YH, Garcia-Garcia C, Serra V, He L, Torres-Lockhart K, Prat A, et al. PI3K inhibition impairs BRCA1/2 expression and sensitizes BRCA-proficient triple-negative breast cancer to PARP inhibition. Cancer Discov. 2012;2:1036–47.
41. Choi YE, Battelli C, Watson J, Liu J, Curtis J, Morse AN, et al. Sublethal concentrations of 17-AAG suppress homologous recombination DNA repair and enhance sensitivity to carboplatin and olaparib in HR proficient ovarian cancer cells. Oncotarget. 2014;5:2678–87.
42. Lim JJ, Yang K, Taylor-Harding B, Wiedemeyer WR, Buckanovich RJ. VEGFR3 inhibition chemosensitizes ovarian cancer stemlike cells through down-regulation of BRCA1 and BRCA2. Neoplasia. 2014;16(343–353):e341-342.
43. Yap TA, Kristeleit R, Michalarea V, Pettitt SJ, Lim JSJ, Carreira S, et al. Phase I Trial of the PARP Inhibitor Olaparib and AKT Inhibitor Capivasertib in Patients with BRCA1/2- and Non-BRCA1/2-Mutant Cancers. Cancer Discov. 2020;10:1528–43.
44. Best OG, Gardiner AC, Majid A, Walewska R, Austen B, Skowronska A, et al. A novel functional assay using etoposide plus nutlin-3a detects and distinguishes between ATM and TP53 mutations in CLL. Leukemia. 2008;22:1456–9.
45. Jimenez-Pascual A, Hale JS, Kordowski A, Pugh J, Silver DJ, Bayik D, et al. ADAMDEC1 Maintains a Growth Factor Signaling Loop in Cancer Stem Cells. Cancer Discov. 2019;9:1574–89.
46. Bharti R, Dey G, Das AK, Mandal M. Differential expression of IL-6/IL-6R and MAO-A regulates invasion/angiogenesis in breast cancer. Br J Cancer. 2018;118:1442–52.
47. Weinstock DM, Nakanishi K, Helgadottir HR, Jasin M. Assaying double-strand break repair pathway choice in mammalian cells using a targeted endonuclease or the RAG recombinase. Methods Enzymol. 2006;409:524–40.
48. Pillay N, Tighe A, Nelson L, Littler S, Coulson-Gilmer C, Bah N, et al. DNA Replication Vulnerabilities Render Ovarian Cancer Cells Sensitive to Poly(ADP-Ribose) Glycohydrolase Inhibitors. Cancer Cell. 2019;35(519–533):e518.
49. Bharti R, Dey G, Ojha PK, Rajput S, Jaganathan SK, Sen R, et al. Diacerein-mediated inhibition of IL-6/IL-6R signaling induces apoptotic effects on breast cancer. Oncogene. 2016;35:3965–75.

Publisher's Note